УДК 546.224-31:547.233:547.477.1 doi: 10.33609/2708-129X.91.3.2025.3-24

SULFUR DIOXIDE INTERACTION WITH MONOETHANOLAMMONIUM AND POLYETHYLENEPOLYAMMONIUM CITRATES AQUEOUS SOLUTIONS PRODUCTS COMPOSITION AND THE RELATIVE STABILITY.

R. E. Khoma*, K. V. Tsyganenko, T. S. Bienkovska, Yu. V. Ishkov, S. V. Vodzinskii

Odessa I.I. Mechnikov National University,
2 Dvoryanska str., 65082 Odessa, Ukraine
**e-mail: rek@onu.edu.ua*

The paper presents the results of pH, redox, and conductometric studies on the acid-base interaction during sulfur dioxide chemisorption by aqueous solutions containing 0.1 mol/L monoethanolammonium **(MEA·1/3CA)** and polyethylenepolyammonium **(PEPA·1/3CA)** citrates, as well as buffer solutions of monoethanolamine – monoethanolammonium citrate **(MEA·1/6CA)**and polyethylenepolyamine – polyethylenepolyammonium citrate **(PEPA·1/6CA)**, in comparison with sodium citrate. The composition of the compounds formed during SO_2 absorption by Na_3Cit, MEA·1/3CA, PEPA·1/3CA, MEA·1/6CA, and PEPA·1/6CA solutions at 273–313 K was determined. For the same amount of absorbed sulfur dioxide, an increase in specific electrical conductivity (æ) with rising temperature was observed in SO_2–Na_3Cit–H_2O and SO_2–MEA·1/3CA–H_2O solutions within the 273–313 K range. However, in the SO_2–MEA·1/3CA–H_2O, SO_2–PEPA·1/3CA–H_2O, SO_2–MEA·1/6CA–H_2O, and SO_2–PEPA·1/6CA–H_2O systems, a decrease in Δæ was noted upon heating to 303 K, which is attributed to their ion-molecular composition.

Based on developed mathematical models, the ion-molecular component composition of SO_2–MEA·1/3CA–H_2O and SO_2–MEA·1/6CA–H_2O solutions was determined at 283–313 K. The concentration and thermodynamic constants for the formation of ionic associates were calculated:
$(\overset{+}{N}H_3CH_2CH_2OH)_2SO_3$, $\{\overset{+}{N}H_3CH_2CH_2OH\}\{HOC_3H_4(COOH)_2(COO^-)\}$ (**Ia**),
$\{\overset{+}{N}H_3CH_2CH_2OH\}_2\{HOC_3H_4(COOH)(COO^-)_2\}$ (**IIa**),
$\{\overset{+}{N}H_3CH_2CH_2OH\}_2\{HOC_3H_4(COOH)_2(COO^-)\}$ (**IIb**),
$\{\overset{+}{N}H_3CH_2CH_2OH\}_3\{HOC_3H_4(COO^-)_3\}$ (**IIIa**),
as well as ion-molecular associates:
$\{\overset{+}{N}H_3CH_2CH_2OH\}\{HOC_3H_4(COOH)_3\}$ (**Ib**),
$\{NH_2CH_2CH_2OH\}_3\{\overset{+}{N}H_3CH_2CH_2OH\}_3\{HOC_3H_4(COO^-)_3\}$ (**IVa**),
$\{NH_2CH_2CH_2OH\}_2\{\overset{+}{N}H_3CH_2CH_2OH\}_4\{HOC_3H_4(COO^-)_3\}$ (**IVb**).

In SO_2–MEA·1/3CA–H_2O solutions, as the temperature increases, bond rearrangement occurs in ionic associates **IIa** and **Ib**, as indicated by the absence of a clear temperature dependence of p β^T_{IIIa}, along with the strengthening of **IIa** and **Ib**. Conversely, in SO_2–MEA·1/6CA–H_2O solutions, increasing temperature leads to the weakening of the bonds in compounds **Ia, IIIa, IVa,** and **IVb**, while in compound **Ib,** the bonds strengthen.

Keywords: sulfur dioxide, ammonium citrates, acid-base interaction, ion associates, ion-molecular associates.

INTRODUCTION. For sanitary air purification from acidic gases (particularly SO_2), absorption and adsorption methods using various chemisorbents are widely used [1, 2]. Previously, the authors [3, 4] studied the acid-base interaction of sulfur dioxide with model aqueous solutions of organic N-containing bases (**AM**), including monoethanolamine (**MEA**) and polyethylenepolyamine (**PEPA**), to develop chemisorbents for acidic gas filtration in respiratory protection [3–5]. To prevent the evaporation of volatile MEA from the surface of impregnated fibrous chemisorbents (**IFCS**) under the flow of a gas-air mixture, polybasic acids (particularly citric acid (**CA**)) were added to the impregnating aqueous solutions based on MEA. This modification enhanced the protective characteristics of IFCS against SO_2 exposure [5]. Additionally, aqueous sodium citrate solutions ($HOC(CH_2COONa)_2COONa$; **Na_3Cit**) have been identified as effective chemisorbents for this gas [6–8].

Methods of pH-, redox- and conductometric titration have been successfully applied to determine the reactivity of model aqueous AM solutions towards SO_2 and CA, allowing for the calculation of their ion-molecular composition and formation constants of weakly dissociated compounds (such as ammonium sulfites, hydrosulfites, pyrosulfites; and ion-molecular complexes) [3, 4, 9].

In [9] the acid-base and electrochemical behavior of Na_3Cit – CA – H_2O, MEA – CA – H_2O, and PEPA – CA – H_2O solutions were analyzed using pH-metric and conductometric data. The study determined the influence of amine type and temperature on the ionic-molecular composition, ionic strength, and structural characteristics of these systems. It also identified key factors (component ratios and temperature) affecting the formation constants of ionic associates. In [10], the influence of water content and **MEA** on the physical and chemical adsorption of sulfur dioxide by **IFCS** samples based on citrate-monoethanolammonium buffer systems was investigated. Competitive adsorption of H_2O and SO_2 by the surface of the indicated **IFCS** was noted. However, no comprehensive data exists in the literature regarding the interaction of sulfur dioxide with ammonium citrates.

Given this gap, the present study aims to determine the composition and relative stability of the products formed during the interaction of sulfur dioxide with aqueous solutions of sodium citrate, monoethanolammonium citrate (**MEA·1/3CA**), and polyethylenepolyammonium citrate (**PEPA·1/3CA**), as well as with buffer solutions of monoethanolamine – monoethanolammonium citrate (**MEA·1/6CA**) and polyethylenepolyamine – polyethylenepolyammonium citrate (**PEPA·1/6CA**). To achieve this goal, a pH, redox, and conductometric study of the above interactions was carried out.

EXPERIMENT AND DISCUSSION OF RESULTS. In this study, monoethanolamine (MEA), sodium citrate (Na_3Cit), and citric acid (CA) of "chemically pure" classification, as well as polyethylenepolyamine (PEPA) (CAS 29320-38-5) without preliminary purification were used. Their characteristics are given in Table 1. Additionally, gaseous sulfur dioxide was supplied from a cylinder. As chemisorbents, aqueous solutions of Na_3Cit, MEA·1/3CA, MEA·1/6CA, PEPA·1/3CA, and PEPA·1/6CA with a Na^+ ion or amine nitrogen concentration of 0.1 mol/L were used. Aqueous solutions of MEA·1/3CA and MEA·1/6CA were prepared by adding a CA solution to an MEA solution at a molar ratio of components

of 1.0:3.0 and 1.0:6.0, respectively. Aqueous solutions of PEPA·1/3CA and PEPA·1/6CA were prepared similarly. The procedure for pH-, redox- and conductometric titration of aqueous solutions with gaseous sulfur dioxide is described in detail in [20].

Figures 1–8 present the pH, redox, and conductometric titration curves for 0.1 mol/L aqueous solutions of Na_3Cit, MEA·1/3CA, PEPA·1/3CA, MEA·1/6CA and PEPA·1/6CA with gaseous sulfur dioxide.

On the integral pH-metric titration curves (Fig. 1, 2) of aqueous solutions of sodium citrates, monoethanolammonium, and polyethylenepolyammonium with gaseous sulfur dioxide, a single jump is observed at the molar ratios $Q(SO_2):Q(Na) = (0.86 \div 0.97):2.00$, $Q(SO_2):Q(N_{MEA}) = (0.92 \div 0.98):2.00$ and $Q(SO_2):Q(N_{PEPA}) = (0.63 \div 0.81):2.00$. These correspond to the peaks on the differential curves (see, for example, Fig. 4a) and contrast with the MEA and PEPA solutions [3], which exhibit two effects.

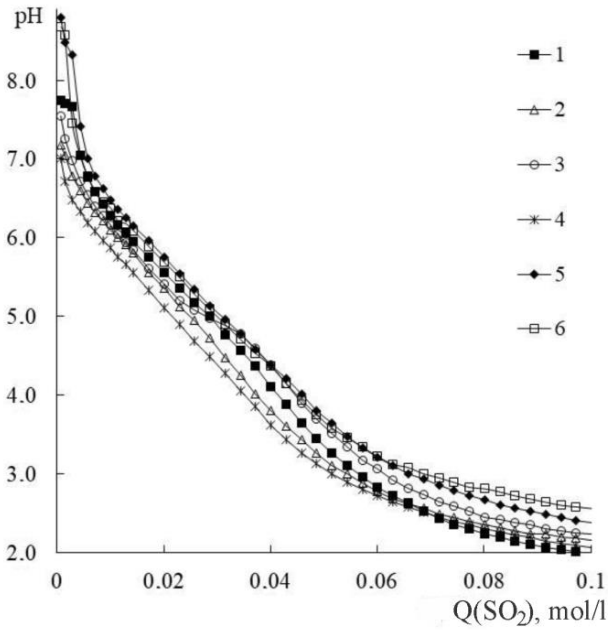

Fig. 1. Integral pH-metric titration curves of a 0.1 mol/L Na_3Cit aqueous solution with gaseous SO_2 at different temperatures (T, K): 273 – 1; 283 – 2; 293 – 3; 298 – 4; 303 – 5; 313 – 6.

This behavior is due to the weakly alkaline nature of the initial citrate solutions (Fig. 1–2; pH 7.61 ÷ 8.82 (Na_3Cit), 6.32 ÷ 6.50 (MEA·1/3CA), and 4.80 ÷ 5.42 (PEPA·1/3CA)). The observed effects on the differential curves occur in an acidic environment (Table 2; pH 3.60 ÷ 3.94 (Na_3Cit), 3.30 ÷ 3.96 (MEA·1/3CA) and 2.81 ÷ 3.74 (PEPA·1/3CA)) and are associated with the formation of hydrosulfites of the corresponding cations. Deviations of the $Q(SO_2):Q(Na)$, $Q(SO_2):Q(N_{MEA})$, and $Q(SO_2):Q(N_{PEPA})$ ratios from the stoichiometry value (1.00:2.00) are due to additional interactions, particularly the stepwise protonation of citrate ions in the specified pH range [9, 20].

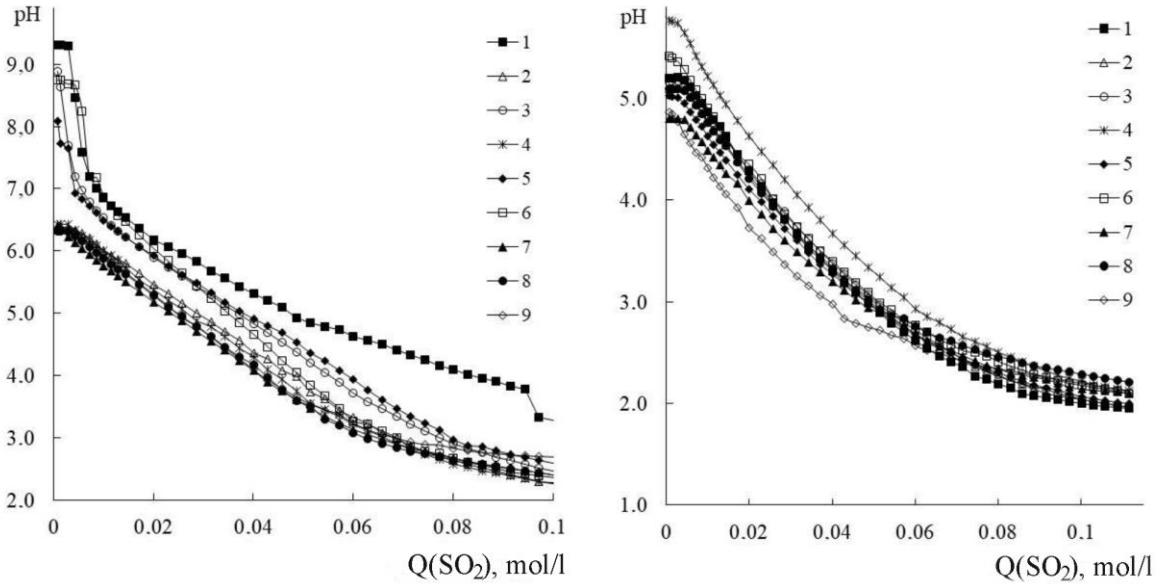

a *b*

Fig. 2. Integral pH-metric titration curves of a 0.1 mol/L MEA·1/3CA (*a*) and PEPA·1/3CA (*b*) aqueous solution with gaseous SO_2 at different temperatures (T, K): 273 – 1; 278 – 2; 283 – 3; 288 – 4; 293 – 5; 298 – 6; 303 – 7; 308 – 8; 313 – 9.

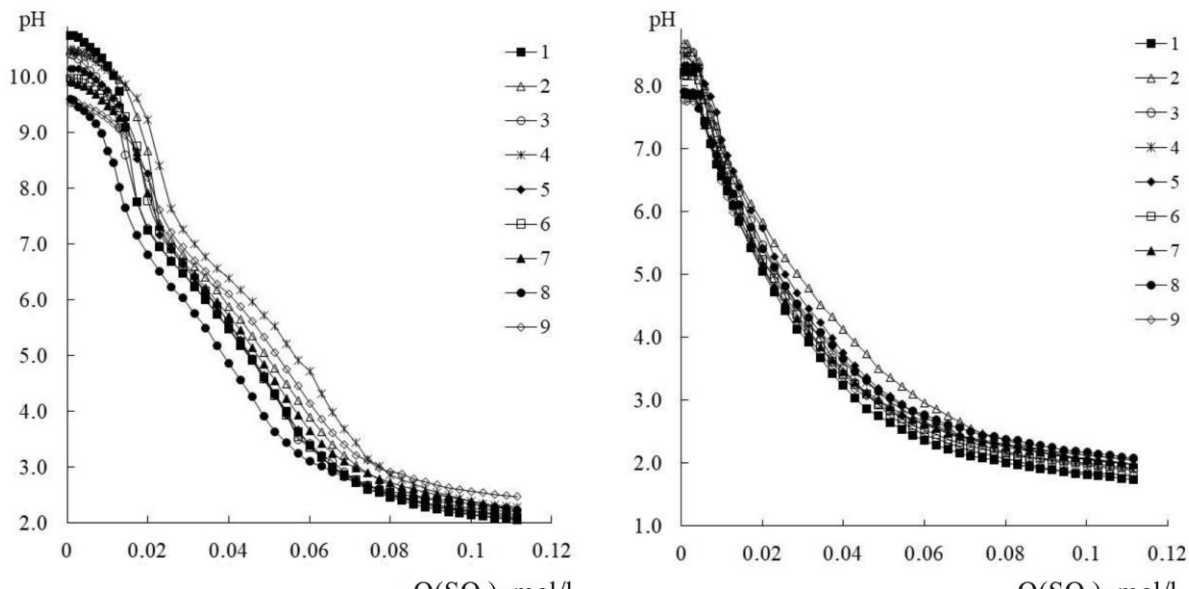

a *b*

Fig. 3. Integral pH-metric titration curves of MEA·1/6CA (*a*) and PEPA·1/6CA (*b*) aqueous solutions with gaseous SO_2 at different temperatures (T, K): 273 – 1; 278 – 2; 283 – 3; 288 – 4; 293 – 5; 298 – 6; 303 – 7; 308 – 8; 313 – 9.

Table 1.

Physicochemical characteristics of the starting compounds.

Name	**Citric acid**	**Sodium citrate**	**Mono-ethanolamine**	**Polyethylene polyamine**
Designation	**CA**	**Na_3Cit**	**MEA**	**PEPA**
Structural formula	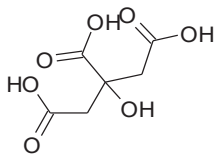	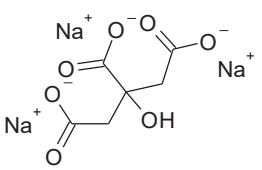	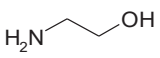	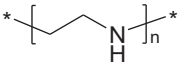
General formula	$HOC_3H_4(COOH)_3$	$HOC_3H_4(COONa)_3$	$NH_2CH_2CH_2OH$	NH_2-$(CH_2CH_2NH)_k$-H
M, g/mol	192.12	258.06	61.08	42.0
pK_a	3.13; 4.76; 6.39 [12]	3.13; 4.76; 6.39 [12, 16]	9.20 [1]	9.21 [18]
Melting point, °C	153 [12, 13]	300 [16]	10.5 [1, 17]	-32.0 [18, 19]
Boiling point, °C	310 [14]	–	170.3 [1, 17]	Decompos. [18, 19]
P, Pa (20 ^{0}C)	$2.21 \cdot 10^{-6}$ [13]	0	53 [1, 17]	<1.33 [18, 19]
lg$P$	-1.64 [15]	-1.72 [16]	-1.31 [1, 17]	-3.67 [18, 19]

In the case of MEA·1/6CA solutions, two jumps are observed on the integral pH-metric curves (Fig. 3a; Table 2) and two maxima on the differential pH-metric curves (e.g., Fig. 4b) at the ratios $Q(SO_2):Q(N_{MEA})$ = (0.34 ÷ 0.52):2.00 and (0.49 ÷ 0.63):1.00. In contrast, PEPA·1/6CA solutions (Fig. 3b; Table 2) exhibit only one effect on the corresponding curves at $Q(SO_2):Q(N_{PEPA})$ = (0.68 ÷ 0.86):2.00. This difference arises from the more alkaline nature of the initial MEA·1/6CA solutions (pH 9.53 ÷ 9.74) compared to PEPA·1/6CA solutions (pH 7.76 ÷ 8.67).

Analyzing the data shown in Fig. 1-3, the pH values of chemisorption systems at 293 K can be arranged in the following sequence:

– for $Q(SO_2) < 0.02$ mol/L MEA·1/6CA > PEPA·1/6CA > MEA·1/3CA > Na_3Cit > PEPA·1/3CA;

– for $0.02 < Q(SO_2) < 0.05$ mol/L MEA·1/6CA > MEA·1/3CA > Na_3Cit > PEPA·1/6CA > PEPA·1/3CA;

– for $0.05 < Q(SO_2) < 0.10$ mol/L MEA·1/3CA > MEA·1/6CA ≥ Na_3Cit > PEPA·1/6CA ≥ PEPA·1/3CA.

These results indicate that at SO_2 concentrations above 0.05 mol/L, solutions based on monoethanolammonium citrate exhibit the highest efficiency in binding this toxicant.

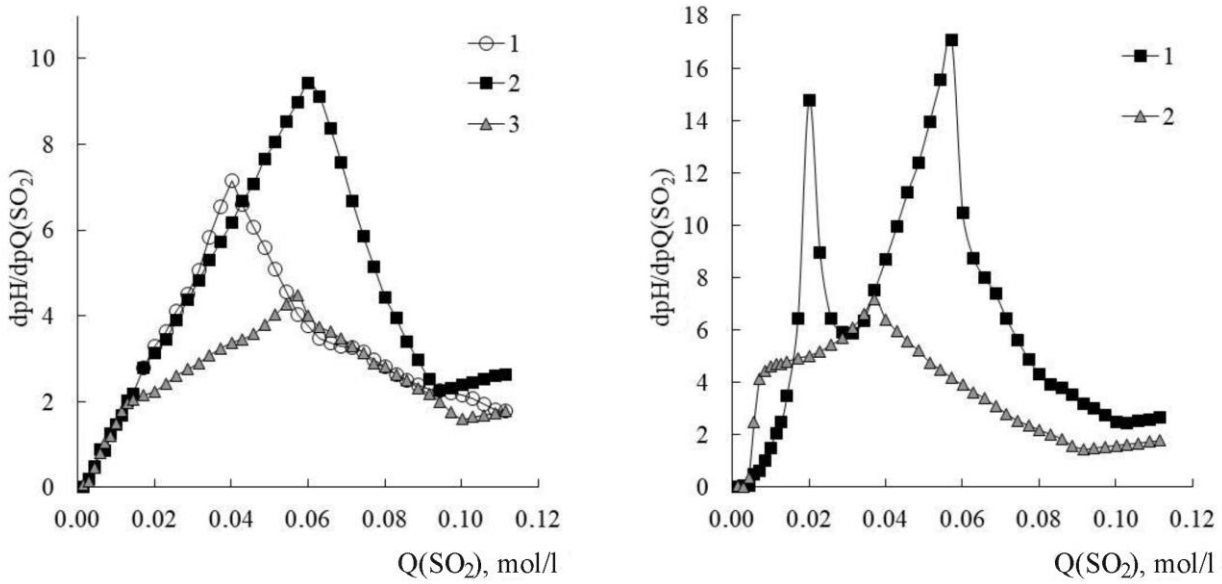

a *b*

Fig. 4. Differential pH-metric titration curves of 0.1 M Na_3Cit (1*a*), MEA·1/3CA (2*a*), PEPA·1/3CA (3*a*), MEA·1/6CA (1*b*) and PEPA·1/6CA (2*b*) aqueous solutions with gaseous SO_2 at 298 K.

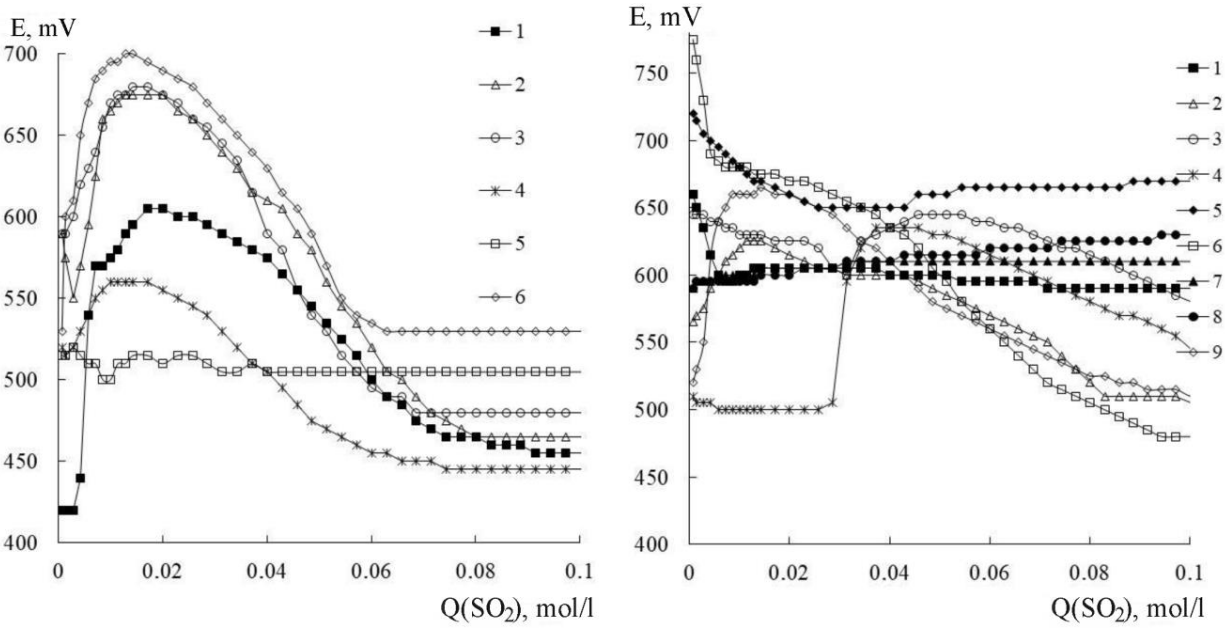

a *b*

Fig. 5. Redox-metric titration curves of 0.1 mol/L Na_3Cit (*a*) and MEA·1/3CA (*b*) aqueous solutions with gaseous SO_2 at different temperatures (T, K): 273 – 1; 283 – 2; 293 – 3; 298 – 4; 303 – 5; 313 – 6.

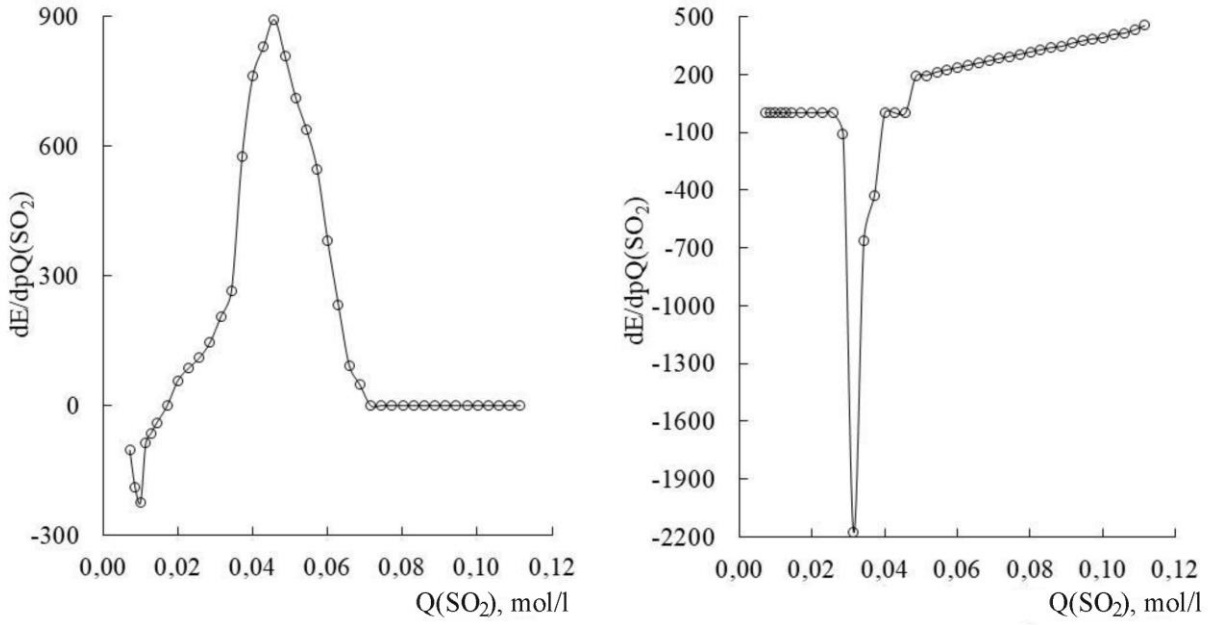

a *b*

Fig. 6. Differential Redox-metric titration curves of 0.1 mol/L Na_3Cit (*a*) and MEA·1/3CA (*b*) aqueous solutions with gaseous SO_2 at 288 K (*b*), and 293 K (*a*).

Negative Δæ values suggest the formation of weakly dissociated compounds in the SO_2 – Na_3Cit – H_2O, SO_2 – MEA·1/3CA – H_2O, and SO_2 – MEA·1/6CA – H_2O systems (Fig. 7 – 9; Table 3). In PEPA-containing solutions, positive Δæ values ($Q(SO_2) > 0.05$ mol/L; T = 273 – 283 K) indicate an increase in the degree of dissociation of existing species (H_2O, $SO_2 \cdot H_2O$, HSO_3^-), the formation of new strongly dissociated compounds, and an increase in the mobility of newly formed ions [3, 11, 20], as discussed below.

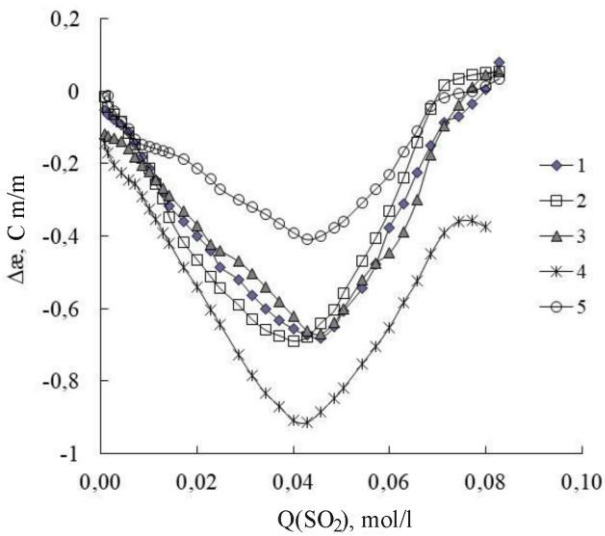

Fig. 7. Conductometric titration curves of 0.1 M Na_3Cit aqueous solutions with gaseous SO_2 at different temperatures (T, K): 273 – 1; 283 – 2; 293 – 3; 303 – 4; 313 – 5.

In the SO_2 – MEA·1/3CA – H_2O system (Fig. 8a; Table 3), the relative decrease in Δæ with increasing sulfur dioxide content up to 0.040 mol/L (at 303, 283 K) and 0.050 mol/L (at 273, 278, 293, and 313 K) is attributed to the formation of monoethanolammonium sulfite, similar to findings in [3, 20]. Further increases in $Q(SO_2)$ are accompanied by a relative increase in the specific electrical conductivity, driven by the formation of monoethanolammonium hydrosulfite and pyrosulfite. As the temperature increases within the 283–303 K range, a relative decrease in Δæ is observed at the same $Q(SO_2)$ values in the 0.01 ÷ 0.05 mol/L region.

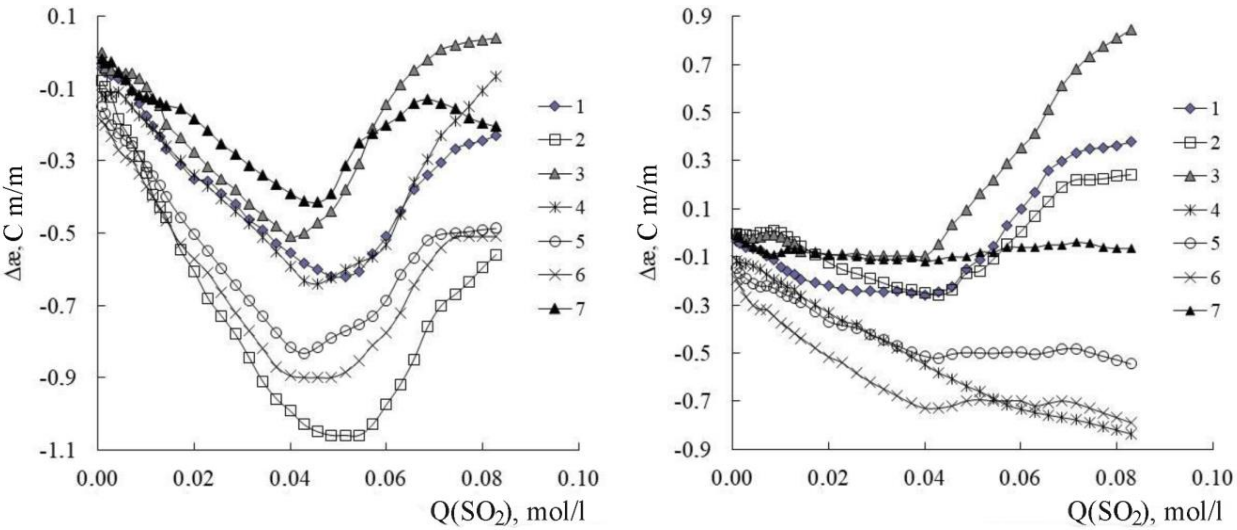

a *b*

Fig. 8. Conductometric titration curves of 0.1 M MEA·1/3CA (*a*), and PEPA·1/3CA (*b*) aqueous solutions with gaseous SO_2 at different temperatures (T, K): 273 – 1; 278 – 2; 283 – 3; 293 – 4; 298 – 5; 303 – 6; 313 – 7.

Table 2.

Characteristics of pH-metric titration curves of Na_3Cit, MEA·1/3CA, PEPA·1/3CA, MEA·1/6CA, and PEPA·1/6CA aqueous solutions with gaseous SO_2.

T, K	1st maximum			2nd maximum		
	$Q(SO_2)$: Q(Na/N)	pH	dpH/dpQ(SO_2)	$Q(SO_2)$: Q(Na/N)	pH	dpH/dpQ(SO_2)
			Na_3Cit			
273	0.429	3.88	8.21	–	–	–
283	0.429	3.60	7.32	–	–	–
293	0.476	3.90	8.56	–	–	–
298	0.404	3.62	7.15	–	–	–
303	0.486	3.81	7.60	–	–	–
313	0.476	3.94	7.49	–	–	–

T, K	1st maximum			2nd maximum		
	$Q(SO_2) : Q(Na/N)$	pH	$dpH/dpQ(SO_2)$	$Q(SO_2) : Q(Na/N)$	pH	$dpH/dpQ(SO_2)$
			MEA·1/3CA			
273	0.472	3.78	13.47	–	–	–
278	0.472	3.78	18.71	–	–	–
283	0.458	3.96	14.51	–	–	–
288	0.472	3.55	14.97	–	–	–
293	0.486	3.30	18.51	–	–	–
298	0.458	3.61	13.33	–	–	–
303	0.472	3.47	10.48	–	–	–
308	0.486	3.30	15.43	–	–	–
313	0.458	3.65	10.15	–	–	–
			PEPA·1/3CA			
273	0.404	3.30	3.73	0.543	2.79	4.26
278	0.315	3.66	3.62	0.515	2.94	4.43
283	0.315	3.74	3.62	0.515	2.97	4.03
288	0.572	3.04	4.48	–	–	–
293	0.458	3.07	3.57	–	–	–
298	0.572	2.82	4.49	–	–	–
303	0.543	2.81	3.41	–	–	–
308	0.515	2.92	4.03	–	–	–
313	0.343	3.16	2.90	–	–	–
			MEA·1/6CA			
273	0.172	7.75	16.92	0.572	3.64	16.61
278	0.200	8.67	8.96	0.601	3.9	14.16
283	0.172	7.75	10.74	0.572	3.5	21.10
288	0.258	7.63	15.05	0.629	4.32	19.80
293	0.200	8.26	18.97	0.543	3.94	15.33
298	0.200	7.77	14.79	0.486	4.58	13.67
303	0.200	7.91	10.91	0.572	3.94	13.02
308	0.129	8.02	8.41	0.486	3.92	12.91
313	0.229	7.61	10.0	0.601	4.15	14.16
313	0.343	3.16	2.90	–	–	–
			PEPA·1/6CA			
273	0.372	3.42	7.48	–	–	–
278	0.486	3.51	8.36	–	–	–
283	0.372	3.68	8.34	–	–	–
288	0.315	4.18	7.25	–	–	–
293	0.372	3.98	7.48	–	–	–
298	0.372	3.61	7.19	–	–	–
303	0.429	3.28	6.01	–	–	–
308	0.404	3.66	6.84	–	–	–
313	0.3432	3.75	6.35	–	–	–

Table 3.

Characteristics of conductometric titration curves of MEA·1/3CA, PEPA·1/3CA, MEA·1/6CA, and PEPA·1/6CA aqueous solutions.

T, K	I-th effect		II-th effect		III-th effect		IV-th effectr	
	$Q(SO_2) : Q(N)$ (*curve shape*)	Δæ, Cm/m	$Q(SO_2) : Q(N)$ (*curve shape*)	Δæ, Cm/m^{-1}	$Q(SO_2) : Q(N)$ (*curve shape*)	Δæ, Cm/m^{-1}	$Q(SO_2) : Q(N)$ (*curve shape*)	Δæ, Cm/m^{-1}
MEA·1/3CA								
273	0.200 (bend)	-0.35	0.510 (bend)	-0.608	0.740 (bend)	-0.276	–	–
278	0.480 (bend)	-1.06	0.540 (bend)	-1.060	0.710 (bend)	-0.760	–	–
283	0.071 (bend)	-0.06	0.400 (min)	-0.510	0.710 (bend)	0.020	–	–
293	0.043 (bend)	-0.114	0.457 (min)	-0.640	0.570 (bend)	-0.565	–	–
298	0.428 (min)	-0.833	0.570 (bend)	-0.729	0.714 (bend)	-0.503	–	–
303	0.400 (bend)	-0.895	0.510 (bend)	-0.885	0.740 (bend)	-0.510	–	–
313	0.171 (bend)	-0.156	0.457 (min)	-0.415	0.686 (bend)	-0.130	–	–
PEPA·1/3CA								
273	0.143 (bend)	-0.192	0.404 (min)	-0.258	0.715 (bend)	0.332	–	–
278	0.072 (max)	0.002	0.429 (min)	-0.259	0.715 (bend)	0.221	–	–
283	0.057 (bend)	-0.017	0.143 (bend)	-0.078	0.400 (bend)	-0.096	0.744 (bend)	0.734
293	0.572 (bend)	-0.717	–	–	–	–	–	–
298	0.572 (bend)	-0.222	0.429 (min)	-0.520	0.486 (bend)	-0.498	0.629 (bend)	-0.506
303	0.400 (min)	-0.729	0.486 (bend)	-0.699	0.686 (bend)	-0.700	–	–
313	0.086 (min)	-0.090	0.129 (max)	-0.070	0.286 (bend)	-0.110	0.400 (bend)	-0.12
MEA·1/6CA								
273	0.110 (max)	0.026	0.486 (min)	-0.38	0.714 (bend)	0.134	–	–
278	0.110 (min)	0.086	0.466 (bend)	-0.38	0.514 (min)	-0.520	0.714 (bend)	-0.030
283	0.100 (max)	0.220	0.486 (min)	-0.21	0.714 (bend)	0.160	–	–
293	0.170 (max)	0.040	0.514 (min)	-0.29	0.714 (bend)	0.140	–	–
298	0.428 (min)	-0.215	0.200 (max)	-0.074	0.486 (min)	-0.480	0.714 (bend)	-0.043
303	0.043 (min)	-0.270	0.710 (max)	-0.24	0.151 (bend)	-0.280	0.540 (bend)	-0.780
313	0.071 (min)	-0.070	0.020 (max)	0.04	0.543 (min)	-0.200	0.628 (bend)	-0.20
PEPA·1/6CA								
273	0.143 (bend)	-0.248	0.468 (min)	-0.432	0.743 (bend)	-0.182	–	–
278	0.071 (bend)	-0.013	0.310 (bend)	-0.236	0.400 (bend)	-0.236	0.743 (bend)	0.434
283	0.100 (bend)	-0.068	0.143 (bend)	-0.015	0.400 (min)	-0.231	0.710 (bend)	0.258
293	0.200 (bend)	-0.313	0.314 (bend)	-0.326	0.428 (min)	-0.381	0.743 (bend)	-0.159
298	0.143 (bend)	-0.364	0.428 (min)	-0.540	0.629 (max)	-0.396	–	–
303	0.400 (bend)	-0.701	0.714 (max)	-0.661	–	–	–	–
313	0.017 (min)	-0.123	0.129 (bend)	-0.129	0.429 (bend)	-0.148	0.571 (bend)	-0.038

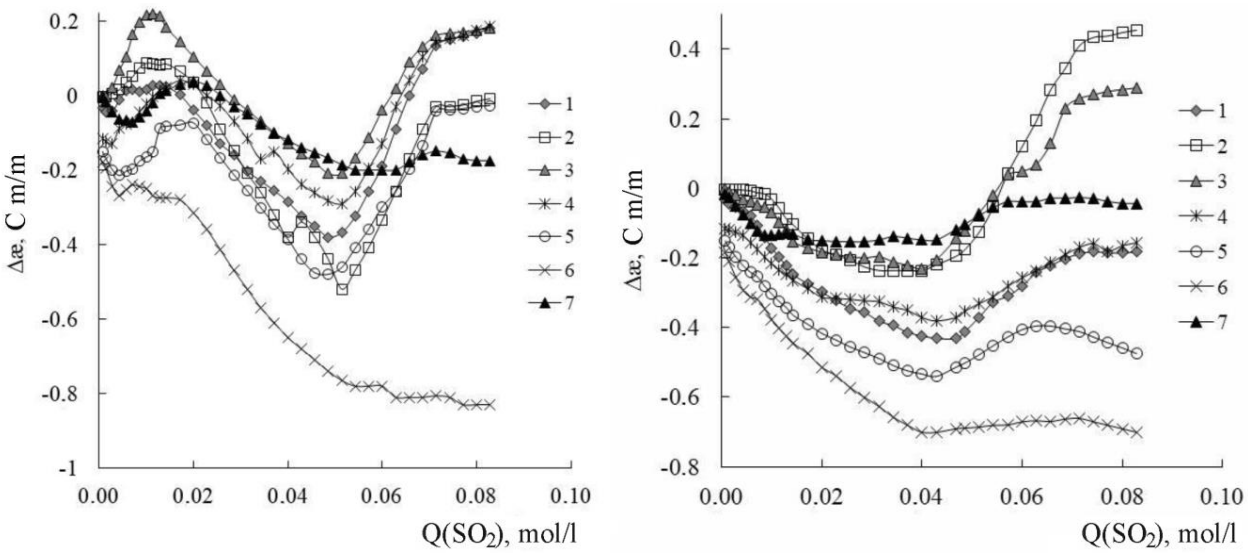

a *b*

Fig. 9. Conductometric titration curves of 0.1 mol/L MEA·1/6CA (*a*) and PEPA·1/6CA (*b*) aqueous solutions with gaseous SO_2 at different temperatures (T, K): T (K): 273 – 1; 278 – 2; 283 – 3; 293 – 4; 298 – 5; 303 – 6; 313 – 7.

At the same $Q(SO_2)$ values, an increase in σ with rising temperature (273–313 K) is observed for SO_2 – Na_3Cit – H_2O and SO_2 – MEA·1/3CA – H_2O solutions. In contrast, in SO_2 – MEA·1/3CA – H_2O, SO_2 – PEPA·1/3CA – H_2O, SO_2 – MEA·1/6CA – H_2O and SO_2 – PEPA·1/6CA – H_2O systems (Figs. 8, 9), Δæ values decrease upon heating within the 283–303 K range. his behavior is attributed to the ionic-molecular composition of the studied systems, which is discussed below.

When sulfur dioxide is absorbed by an MEA·1/6CA solution, Δæ acquires positive values (Fig. 9a) only in specific sections of the $\Delta æ = f(Q(SO_2))$ curves at: 273 K ($0.005 < Q(SO_2) < 0.020$ mol/L), 278 K ($0.002 < Q(SO_2) < 0.020$ mol/L), 283 K ($0.002 < Q(SO_2) < 0.030$ mol/L), 293 K ($0.012 < Q(SO_2) < 0.025$ mol/L) and 313 K ($0.013 < Q(SO_2) < 0.025$ mol/L). Under other experimental conditions, $\Delta æ \leq 0$ Cm·m^{-1}. For PEPA·1/6CA solutions, Δæ values remain negative (Fig. 9b) during SO_2 chemisorption, except at T = 278 and 283 K (curves 2 and 3) when $Q(SO_2):Q(N) \geq 0.55$.

Unlike pH-metric curves (Fig. 3), conductometric curves (Fig. 9; Table 3) exhibit three or four effects. When sulfur dioxide is introduced into the MEA·1/6CA solution, a decrease in Δæ is observed within $0.020 < Q(SO_2) < 0.050$ mol/L across the studied temperature range (Fig. 9a). Further addition of SO_2 leads to a Δæ increase up to $Q(SO_2) \approx 0{,}070$ mol/L (except at T = 293 K), after which the $\Delta æ = f(Q(SO_2))$ dependencies reach stationary regions.

The addition of SO_2 to the PEPA·1/6CA solution leads to a decrease in Δæ within $0.010 < Q(SO_2) < 0.040$ mol/L across the studied

temperature range (Fig. 9b). When $Q(SO_2)$ exceeds (0.040 ÷ 0.045 mol/L), Δæ values begin to increase.

Each Δæ = $f(Q(SO_2))$ curve for SO_2 chemisorption in the studied solutions at a given temperature exhibits distinct effects (Fig. 9; Table 3).

The uniformity of acid-base and electrochemical behavior in solutions containing sodium, monoethanolammonium, and polyethylenepolyammonium citrates is confirmed by the overlapping initial sections of the $dpH/dpQ(SO_2)$ – $Q(SO_2)$ and Δæ – $Q(SO_2)$ curves (Fig. 4, 10).

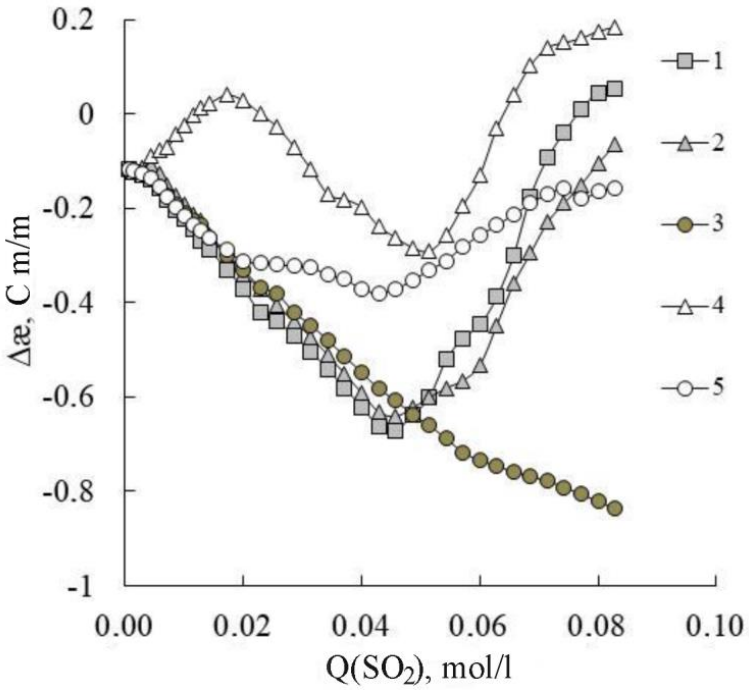

Fig. 10. Conductometric titration curves of 0.1 mol/l Na_3Cit (1), MEA·1/3CA (2) and PEPA·1/3CA (3) MEA·1/6CA (4), and PEPA·1/6CA (5) aqueous solutions with gaseous SO_2 at 293 K.

Physicochemical models of SO_2 interaction with MEA – CA – H_2O and PEPA – CA – H_2O solutions.

According to [9], in aqueous MEA·1/3CA solutions, the following processes take place: water autoprotolysis (reaction 1), MEA protonation (reaction 2), and stepwise dissociation of CA (reactions 3–5). Additionally, the formation of ionic associates occurs:

$\{\overset{+}{N}H_3CH_2CH_2OH\}\{HOC_3H_4(COOH)_2(COO^-)\}$ (**Ia**),
$\{\overset{+}{N}H_3CH_2CH_2OH\}_2\{HOC_3H_4(COOH)(COO^-)_2\}$ (**IIa**),
$\{\overset{+}{N}H_3CH_2CH_2OH\}_2\{HOC_3H_4(COOH)_2(COO^-)\}$ (**IIb**),
$\{\overset{+}{N}H_3CH_2CH_2OH\}_3\{HOC_3H_4(COO^-)_3\}$ (**IIIa**), as well as the ionic-molecular associate
$\{\overset{+}{N}H_3CH_2CH_2OH\}\{HOC_3H_4(COOH)_3\}$ (**Ib**) (reactions 6–10).

$$2H_2O \rightleftarrows H_3O^+ + OH^- \quad (1)$$

$$NH_2CH_2CH_2OH + H_3O^+ \overset{1/Ka}{\rightleftarrows} \overset{+}{N}H_3CH_2CH_2OH + H_2O \quad (2)$$

$$HOC_3H_4(COOH)_3 + H_2O \rightleftarrows HOC_3H_4(COOH)_2COO^- + H_3O^+ \quad (3)$$

$$HOC_3H_4(COOH)_2COO^- + H_2O \rightleftarrows HOC_3H_4(COOH)(COO^-)_2 + H_3O^+ \quad (4)$$

$$HOC_3H_4(COOH)(COO^-)_2 + H_2O \rightleftarrows HOC_3H_4(COO^-)_3 + H_3O^+ \quad (5)$$

$$\overset{+}{N}H_3CH_2CH_2OH + HOC_3H_4(COOH)_2(COO^-) \overset{\beta_{Ia}}{\rightleftarrows} \rightleftarrows \{\overset{+}{N}H_3CH_2CH_2OH\}\{HOC_3H_4(COOH)_2(COO^-)\} \quad (6)$$

$$\overset{+}{N}H_3CH_2CH_2OH + HOC_3H_4(COOH)_3 \overset{\beta_{Ib}}{\rightleftarrows} \rightleftarrows \{\overset{+}{N}H_3CH_2CH_2OH\}\{HOC_3H_4(COOH)_3\} \quad (7)$$

$$2\overset{+}{N}H_3CH_2CH_2OH + HOC_3H_4(COOH)(COO^-)_2 \overset{\beta_{IIa}}{\rightleftarrows} \rightleftarrows \{\overset{+}{N}H_3CH_2CH_2OH\}_2\{HOC_3H_4(COOH)(COO^-)_2\} \quad (8)$$

$$2\overset{+}{N}H_3CH_2CH_2OH + HOC_3H_4(COOH)_2(COO^-) \overset{\beta_{IIb}}{\rightleftarrows} \rightleftarrows \{\overset{+}{N}H_3CH_2CH_2OH\}_2\{HOC_3H_4(COOH)_2(COO^-)\} \quad (9)$$

$$3\overset{+}{N}H_3CH_2CH_2OH + HOC_3H_4(COO^-)_3 \overset{\beta_{IIIa}}{\rightleftarrows} \rightleftarrows \{\overset{+}{N}H_3CH_2CH_2OH\}_3\{HOC_3H_4(COO^-)_3\} \quad (10)$$

When SO_2 interacts with MEA·1/3CA – H_2O solutions, reactions 11–18 occur, leading to the formation of sulfur dioxide hydrate, sulfite, hydrosulfite, and pyrosulfite anions, as well as monoethanolammonium sulfite (**IS**), hydrosulfite (**IIS**), and pyrosulfite (**IIIS**) [3, 20].

$$SO_2^r \rightleftarrows SO_2^p \quad (11)$$

$$SO_2^p + H_2O \rightleftarrows SO_2\cdot H_2O \quad (12)$$

$$SO_2\cdot H_2O + H_2O \overset{K_1}{\rightleftarrows} H_3O^+ + HSO_3^- \quad (13)$$

$$2HSO_3^- \overset{K}{\rightleftarrows} S_2O_5^{2-} + H_2O \quad (14)$$

$$HSO_3^- + H_2O \overset{K_2}{\rightleftarrows} H_3O^+ + SO_3^{2-}, \quad (15)$$

when SO_2^r, SO_2^p – sulfur dioxide in the gas phase and dissolved in water, respectively.

$$2NH_2CH_2CH_2OH + SO_2\cdot H_2O \overset{\beta_{IS}}{\rightleftarrows} (NH_3CH_2CH_2OH)_2SO_3 \quad (16)$$

$$NH_2CH_2CH_2OH + SO_2\cdot H_2O \overset{\beta_{IIS}}{\rightleftarrows} \rightleftarrows (NH_3CH_2CH_2OH)HSO_3 \quad (17)$$

$$2NH_2CH_2CH_2OH + 2(SO_2\cdot H_2O) \overset{\beta_{IIIS}}{\rightleftarrows} \rightleftarrows (NH_3CH_2CH_2OH)_2S_2O_5 + H_2O \quad (18)$$

SO_2 – Na_3Cit – H_2O solutions

Based on [3, 4, 11, 20], the interaction of citrate ions with SO_2 hydrate results in the formation of sulfite and hydrocitrate anions (reaction 19). Additionally, the reaction of sulfite ions with SO_2 in water leads to the formation of hydrosulfite ions (reaction 20). These processes are responsible for the initial jumps observed on the pH-metric titration curves of sodium citrate aqueous solutions (Fig. 1).

$$HOC_3H_4(COO^-)_3 + SO_2\cdot H_2O + OH^- \rightarrow SO_3^{2-} + HOC_3H_4(COOH)(COO^-)_2 + H_2O \quad (19)$$

$$SO_3^{2-} + SO_2\cdot H_2O \rightarrow 2HSO_3^- \quad (20)$$

When $HOC_3H_4(COOH)(COO^-)_2$ ions interact with SO_2, hydrosulfite and dideprotonated citrate anions are formed (reaction 21). Hydrosulfite ions are also generated through the dissociation of «sulfuric» acid (reaction 13). Reactions 13 and 21 are responsible for the second jumps on the pH-metric titration curves and the minima on the conductometric curves. Additionally, at pH 4.5–6.0, hydrosulfite ion dimerization (reaction 14) leads to the formation of pyrosulfite ions, causing the first jumps on the redox-metric curves (Fig. 5*a*).

$$SO_2\cdot H_2O + HOC_3H_4(COOH)(COO^-)_2 \rightarrow HSO_3^- + HOC_3H_4(COOH)_2(COO^-) \quad (21)$$

SO_2 – MEA·1/3CA – H_2O solutions

The replacement of sodium citrate with monoethanolammonium citrate in chemisorption solutions introduces additional reactions 22–23. Alongside the reactions occurring in the SO_2 – Na_3Cit – H_2O system, this system also allows for the interaction of the ionic associate (monoethanolammonium citrate) with SO_2, which is responsible for the first jumps on the pH-metric curves (Fig. 2*a*). At pH 4,0–6,0, the reaction between SO_2 and monoethanolammonium cations in water produces an ionic associate – ammonium sulfite (reaction 23), leading to minima on the conductometric curves (Fig. 8 *a*).

$$\{\overset{+}{N}H_3CH_2CH_2OH\}_3\{HOC_3H_4(COO^-)_3\} + SO_2\cdot H_2O \rightarrow \{\overset{+}{N}H_3CH_2CH_2OH\}_2(SO_3^{2-}) + \overset{+}{N}H_3CH_2CH_2OH + HOC_3H_4(COOH)_2(COO^-) \quad (22)$$

$$2\overset{+}{N}H_3CH_2CH_2OH + SO_2\cdot H_2O + 2H_2O \rightarrow \{\overset{+}{N}H_3CH_2CH_2OH\}_2(SO_3^{2-}) + 2H_3O^+ \quad (23)$$

The multicomponent nature of SO_2 – MEA·1/3CA – H_2O solutions, resulting from the formation of H-bonded ionic associates, leads to variations in redox-metric curve shapes at different temperatures.

SO_2 – PEPA·1/3CA – H_2O solutions.

The interaction of SO_2 with polyethylenepolyammonium citrate (reaction 24) leads to the formation of polyethylenepolyammonium sulfite, polyethylenepolyamine, and dihydrocitrate ions. This process causes jumps in the pH-metric curves (Fig. 2 *b*) and breaks or minima in the conductometric curves (Fig. 8 *b*).

$$\{\overset{+}{N}H_3(CH_2CH_2\overset{+}{N}H_2)_kH\}_3\{HOC_3H_4(COO^-)_3\}_{k+1} + (k{+}1)SO_2\cdot H_2O + H_2O \rightarrow \{\overset{+}{N}H_3(CH_2CH_2\overset{+}{N}H_2)_kH\}_2(SO_3^{2-})_{k+1} + NH_2(CH_2CH_2NH)_kH + (k{+}1)HOC_3H_4(COOH)_2(COO^-) + H_3O^+ \quad (24)$$

The component composition of SO_2 – MEA·1/3CA – H_2O solutions.

Considering the law of mass action (equations 1 – 18), along with the material balance equations for nitrogen (25), citrates (26), and sulfur (27), and the electroneutrality condition (28), a system of mathematical equations (1–18, 25–28) is established.

$$Q_N = [NH_2CH_2CH_2OH] + [\overset{+}{N}H_3CH_2CH_2OH] + C_{Ia} + C_{Ib} + 2C_{IIa} + 2C_{IIb} + 3C_{IIIa} + 2C_{IS} + C_{IIS} + 2C_{IIIS} \quad (25)$$

$$Q_{Cit} = [HOC_3H_4(COOH)_3] + [HOC_3H_4(COOH)_2COO^-] + [HOC_3H_4(COOH)(COO^-)_2] + [HOC_3H_4(COO^-)_3] + C_{Ia} + C_{Ib} + C_{IIa} + C_{IIb} + C_{IIIa} \quad (26)$$

$$Q(SO_2) = [SO_2 \cdot H_2O] + [HSO_3^-] + 2[S_2O_5^{2-}] + [SO_3^{2-}] + C_{IS} + C_{IIS} + 2C_{IIIS} \quad (27)$$

$$[H^+] + [\overset{+}{N}H_3CH_2CH_2OH] + C_{Ib} + C_{IIb} = [OH^-] + [HSO_3^-] + 2[S_2O_5^{2-}] + 2\cdot[SO_3^{2-}] \quad (28)$$

where $C_{IS} = [(NH_3CH_2CH_2OH)_2SO_3]$, $C_{IIS} = [(NH_3CH_2CH_2OH)HSO_3]$,
$C_{IIIS} = [(NH_3CH_2CH_2OH)_2S_2O_5]$, $C_{Ia} = [\{\overset{+}{N}H_3CH_2CH_2OH\}\{HOC_3H_4(COOH)_2(COO^-)\}]$,
$C_{Ib} = [\{\overset{+}{N}H_3CH_2CH_2OH\}\{HOC_3H_4(COOH)_3\}]$,
$C_{IIa} = [\{\overset{+}{N}H_3CH_2CH_2OH\}_2\{HOC_3H_4(COOH)(COO^-)_2\}]$,
$C_{IIb} = [\{\overset{+}{N}H_3CH_2CH_2OH\}_2\{HOC_3H_4(COOH)_2(COO^-)\}]$,
$C_{IIIa} = [\{\overset{+}{N}H_3CH_2CH_2OH\}_3\{HOC_3H_4(COO^-)_3\}]$.

Solving this system using pH-metric data (Fig. 2 *a*) and incorporating the pK_a values of CA and MEA (Table 1) enabled the calculation of the component composition of SO_2 – MEA·1/3CA – H_2O solutions (Fig. 11).

According to the obtained data, as $Q(SO_2)$ increases from $1.4\cdot10^{-3}$ to $1.4\cdot10^{-2}$ mol/L, a rise in the relative content of monoethanolammonium cation (curve 6) is observed due to the dissociation of ionic associate **IIIa** (Fig. 11, curves 4, 7). In the region where ionic associate **IIIa** and ionic-molecular associate **IIb** form (Table 2), the total SO2 content increases the cation's partial binding into ammonium sulfite **IS** (curve 8). When ionic associate **IIb** transitions into compound **IIa** $Q(SO_2) > 0.26$ mol/L, the relative content of IS decreases (curve 8), while the binding of monoethanolamine and citrate in **IIa** increases sharply (curves 4 and 7). Across the calculated section of the pH = $f(Q(SO_2))$ curve, a rise in the molar fraction of hydrosulfite ions (curve 9; $Q(SO_2) > 0.01$ mol/L) is observed, along with a decrease in ammonium sulfite content (curve 10) relative to the total SO_2 concentration. The relative content of SO_2 hydrate, sulfite, and pyrosulfite ions, as well as free MEA, does not exceed 0.7%.

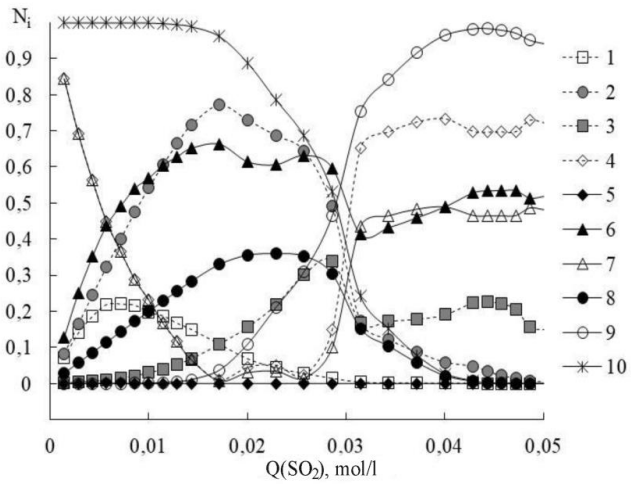

Fig. 11. Partial distribution diagrams of different forms of interaction in the SO_2 – MEA·1/3CA – H_2O system depending on Q_{SO_2} at 293 K. N_i – molar fraction of Cit^{3-} (1), $HCit^{2-}$ (2), H_2Cit^- (3), $C_{IIa} + C_{IIb} + C_{IIIa}$. (4, 7), $NH_2CH_2CH_2OH$ (5), $\overset{+}{N}H_3CH_2CH_2OH$ (6), C_{IS} (8, 10), HSO_3^-(9) relative to the total content of citrates (1–4), nitrogen (5–8) and sulfur (9, 10).

The concentration constants for the formation of ionic associates (β_{IIIS}, $\beta_{Ia} - \beta_{IIIa}$, $\beta_{Ib,}$ and β_{IIb}) have been calculated. Under the experimental conditions, these formation constants exceed 10.

The concentration and thermodynamic constants (β_{IIIS}) for ammonium sulfite formation in SO_2–MEA·1/3CA–H_2O solutions are nearly identical to those in SO_2 – MEA solutions [3, 20]. The dependences of $p\beta_i$ (for compounds **Ib**, **IIa,** and **IIIa**) on ionic strength (μ, M) follow a linear relationship (equation 29), whereas the dependence of $p\beta_{IIb} = f(\mu)$ is more complex (equation 30). The parameters of these equations are provided in Table 4.

$$p\beta_i = A_i + B_i \cdot \mu \quad (29)$$

$$p\beta_{IIb} = A_i + B_i \cdot \mu^{0,5} + C_i \cdot \mu \quad (30)$$

By definition [21], the coefficients A_i in equations 29 and 30 represent the negative decimal logarithms of the conditional thermodynamic constants ($\beta_{Ia} - \beta_{IIIa}$). As temperature increases, bond rearrangements occur in ionic associates **IIa**, **IIIa,** and compound **Ib**, as indicated by the lack of a clear dependence of $p\beta^T_{IIIa}$= f(T). Additionally, compounds **IIa** and **Ib** exhibit increased stability, as reflected in the A_i values of equation 29 (Table 4).

Table 4.

The values of the coefficients A_i, B_i in equation (29) for compounds Ib, IIa, and IIIa, and A_i, B_i, C_i in equation (30) for associate IIb in SO_2 – MEA·1/3CA – H_2O solutions *

T, K	A_i	B_i	R^2	$Q(SO_2):Q_N$
		IIIa		
288	-12.53	28.5	0.9142	0.0715÷0.172
293	-16.16	41.93	0.9384	0.0715÷0.129
303	-9.078	16.76	0.9735	0.0572÷0.257
313	-15.10	38.30	0.9492	0.0572÷0.486
		IIa		
283	-5.55	9.18	0.9868	0.072÷0.143
293	-8.10	21.6	0.9690	0.286÷0.515
		Ib		
283	-17.44	69.80	0.9839	0.400÷0.515
288	-20.24	87.86	0.9653	0.343÷0.458
303	0.05	0	–	0.315
		IIb		
	A_i	B_i	C_i	R^2	$Q(SO_2):Q_N$
283	-21.11	115.72	-191.1	0.9900	0.172÷0.372
288	-13.28	63.59	-88.61	0.9993	0.200÷0.315
293	-9.083	0	23.97	0.7959	0.172÷0.257
303	-1.730	0	0	–	0.286

*R^2 is the value of the approximation reliability.

With rising temperature, the absolute $p\beta^{T}_{IIb}$ values decrease, following a relationship described by equation 31 within the 283–303 K range.

$$p\beta^{T}_{IIb} = 264{,}15 - 88312/T, \quad (31)$$

where T is the absolute temperature, K.

Composition of SO_2 – MEA·1/6CA – H_2O solutions

For MEA·1/6CA solutions, in addition to reactions 1–24, there is also the potential formation of ion-molecular associates **IVa** and **IVb**, as described by equations 32 and 33.

$$3NH_2CH_2CH_2OH + 3\overset{+}{N}H_3CH_2CH_2OH + HOC_3H_4(COO^-)_3 \overset{\beta_{IVa}}{\rightleftarrows} \rightleftarrows \{NH_2CH_2CH_2OH\}_3\{\overset{+}{N}H_3CH_2CH_2OH\}_3\{HOC_3H_4(COO^-)_3\}, \quad (32)$$

$$2NH_2CH_2CH_2OH + 4\overset{+}{N}H_3CH_2CH_2OH + HOC_3H_4(COO^-)_3 \overset{\beta_{IVb}}{\rightleftarrows} \rightleftarrows \{NH_2CH_2CH_2OH\}_2\{\overset{+}{N}H_3CH_2CH_2OH\}_4\{HOC_3H_4(COO^-)_3\}. \quad (33)$$

Based on experimental data (Fig. 3a) and a mathematical model that incorporates the law of mass action (equations 1–18, 32, 33), along with the material balance equations for nitrogen (34), citrates (35), and sulfur (27), as well as the electroneutrality condition (36), the ionic-molecular composition of SO_2–MEA·1/6CA–H_2O solutions was determined (for example, Fig. 12).

$$Q_N = [NH_2CH_2CH_2OH] + [\overset{+}{N}H_3CH_2CH_2OH] + C_{Ia} + C_{Ib} + 2C_{IIa} + 2C_{IIb} + 3C_{IIIa} + 2C_{IS} + C_{IIS} + 2C_{IIIS} + 6C_{IVa} + 6C_{IVb} \quad (34)$$

$$Q_{Cit} = [HOC_3H_4(COOH)_3] + [HOC_3H_4(COOH)_2COO^-] + [HOC_3H_4(COOH)(COO^-)_2] + [HOC_3H_4(COO^-)_3] + C_{Ia} + C_{Ib} + C_{IIa} + C_{IIb} + C_{IIIa} + C_{IVa} + C_{IVb} \quad (35)$$

$$[H^+] + [\overset{+}{N}H_3CH_2CH_2OH] + C_{Ib} + C_{IIb} + C_{IVb} = [OH^-] + [HSO_3^-] + 2[S_2O_5^{2-}] + 2\cdot[SO_3^{2-}] \quad (36)$$

де $C_{IVa} = \{NH_2CH_2CH_2OH\}_3\{\overset{+}{N}H_3CH_2CH_2OH\}_3\{HOC_3H_4(COO^-)_3\}$,
$C_{IVb} = \{NH_2CH_2CH_2OH\}_2\{\overset{+}{N}H_3CH_2CH_2OH\}_4\{HOC_3H_4(COO^-)_3\}$.

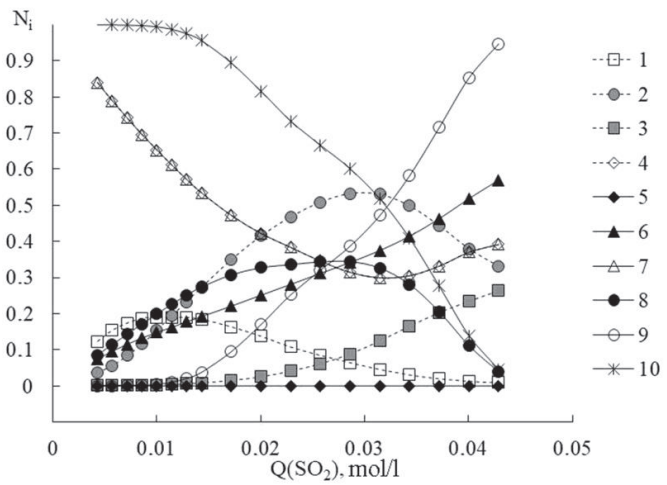

Fig. 12. Partial distribution diagrams of different forms of interaction in the SO_2–MEA·1/6CA–H_2O system depending on Q_{SO_2} at 293 K. Ni – molar fraction of Cit^{3-} (1), $HCit^{2-}$ (2), H_2Cit^- (3), C_{IVa}– (4, 7), $NH_2CH_2CH_2OH$ (5), $\overset{+}{N}H_3CH_2CH_2OH$ (6), C_{IS} (8, 10), HSO_3^- (9) relative to the total content of citrates (1–4), nitrogen (5–8) and sulfur (9, 10).

According to the calculations (Fig. 12), the chemisorption of sulfur dioxide by an MEA·1/6CA aqueous solution occurs due to its binding to monoethanolammonium sulfite **IS** (curve 10) at $Q(SO_2) < 0.0572$ mol/L, following reaction 37. This process is accompanied by:

$$2\{NH_2CH_2CH_2OH\}_3\{\overset{+}{N}H_3CH_2CH_2OH\}_3\{HOC_3H_4(COO^-)_3\} + 3SO_2\cdot H_2O \rightarrow 3(NH_3CH_2CH_2OH)_2SO_3 + 2HOC_3H_4(COO^-)_3 + 6\overset{+}{N}H_3CH_2CH_2OH \quad (37)$$

With further SO_2 addition, the relative content of hydrosulfite anions (curve 9) and monoethanolammonium cations (curve 6) increases due to reaction 38.

$$(NH_3CH_2CH_2OH)_2SO_3 + SO_2\cdot H_2O \rightarrow 2\overset{+}{N}H_3CH_2CH_2OH + 2HSO_3^- \quad (38)$$

In this case:

The mole fraction of the **IS** compound relative to total nitogen (curve 8) reaches a maximum at $Q(SO_2):Q_N = 1.0:4.0$;

The mole fraction of citrate anions (curve 1) reaches a maximum at $Q(SO_2):Q_N = 1.0:10.0$, accompanied by partial protonation of citrate anions with the formation of $HOC_3H_4(COOH)(COO^-)_2$ (curve 2) and dihydrocitrate anions (curve 3).

The relative content of $HOC_3H_4(COOH)(COO^-)_2$ (curve 2) reaches a maximum at $Q(SO_2) = 0.0286$ mol/L, while $HOC_3H_4(COOH)_2COO^-$ (curve 3) increases throughout the studied range.

The content of unbound MEA (as a free base), undissociated CA, sulfite and pyrosulfite anions, and $SO_2\cdot H_2O$ does not exceed 0.02 relative units. Notably, ionic associates **IIa** and **IIb** are not formed during the chemisorption of SO_2 in the studied concentration ($Q(SO_2)$) and temperature ranges, unlike in the MEA·1/3CA solution.

The concentration dependences $\mu = f(Q(SO_2))$ exhibit complex behavior due to the multicomponent nature of the chemisorption system during SO_2 absorption (at 283–288 and 298–313 K). However, at 293 K, only the ion-molecular complex **IVa** is formed between MEA and CA, leading to a linear dependence:

$$\mu = 0{,}0177 + 1{,}0261\cdot Q(SO_2); \quad n = 14;\ R^2 = 0{,}9940. \quad (39)$$

Using the obtained component composition data for SO_2–MEA·1/6CA – H_2O solutions, the concentration constants for the formation of compounds **IIIS**, **Ia**, **Ib**, **IIIa**, **Iva**, and **IVb** were calculated. The dependence $p\beta_{IIb} = f(\mu)$ is described by equation 29, with parameters provided in Table 5.

With increasing temperature, bond weakening is observed in compounds **Ia**, **IIIa**, **IVa** and **IVb**, as indicated by an increase in $p\beta_i$ values, which are numerically equal to the A_i coefficients in equation 29 (Table 5). Conversely, the stability of complex **Ib** increases. The concentration and thermodynamic constants β_{IIIS} for SO_2–MEA·1/6CA–H_2O and SO_2–MEA·1/3CA–H_2O solutions show no significant difference compared to SO_2 – MEA solutions [3, 20].

Table 5.

The values of the A_i, B_i coefficients in equation (29) for compounds Ia, Ib, IIIa, IVa, and IVb in SO_2–MEA·1/6CA–H_2O in solutions*

T, K	A_i	B_i	R^2	$Q(SO_2):Q_N$
		Ia		
303	-5,44	79,27	0,9954	0,315÷0,458
313	19,11	-274,7	0,9890	0,286÷0,400
		Ib		
283	-3,94	6,63	0,9895	0,315÷0,949
288	-5,08	-9,78	0,9741	0,257÷0,486
		IIIa		
288	-17,33	-102,56	0,9978	0,0715÷0,200
313	-6,873	41,14	0,9995	0,0286÷0,143
		IVa		
293	-12,16	-45,31	0,9885	0,014÷0,529
313	22,835	-382	0,8303	0,172÷0,257
		IVb		
283	-18,14	15,30	0,9920	0,072÷0,286
303	18,23	-377,0	0,9935	0,175÷0,263

*R^2 – the value of the approximation confidence.

CONCLUSIONS.

This study, based on pH, redox, and conductometric analyses, evaluates the acid-base interaction during the chemisorption of sulfur dioxide by aqueous solutions of monoethanolammonium and polyethylenepolyammonium citrates in comparison with sodium citrate.

The composition and relative stability of the reaction products formed during SO_2 interaction with aqueous solutions of Na_3Cit, MEA·1/3CA, PEPA·1/3CA, MEA·1/6CA, and PEPA·1/6CA were determined. It was shown that in the presence of ammonium citrates (MEA and PEPA), the following species are formed: ionic associates **Ia, IIa, IIb, IIIa**; ion-molecular associates **Ib, IVa, IVb**; and ammonium sulfites, hydrosulfites, and pyrosulfites. The component composition, as well as the concentration and thermodynamic constants of these associates, were calculated. In SO_2–MEA·1/3CA–H_2O solutions, increasing temperature enhances the relative stability of compounds **IIa** and **Ib**. In SO_2–MEA·1/6CA–H_2O solutions, the stability of compounds **Ia, IIIa, IVa** and **IVb** decreases, while **Ib** increases with rising temperature. Adding CA to the SO_2–MEA–H_2O system in MEA:CA ratios of 3:1 and 6:1 has no significant effect on the concentration and thermodynamic constants of ammonium sulfites formation.

The results obtained will be applied in the development of chemosorbents for respiratory protection.

ACKNOWLEDGEMENT. The work was carried out within the framework of the state budget theme "Scientific principles of creating hybrid fibrous filter materials for personal and collective protection equipment", state registration number: 0124U000930.

СКЛАД ТА ВІДНОСНА СТІЙКІСТЬ ПРОДУКТІВ ВЗАЄМОДІЇ ДІОКСИДУ СІРКИ З ВОДНИМИ РОЗЧИНАМИ ЦИТРАТІВ МОНОЕТАНОЛАМОНІЮ ТА ПОЛІЕТИЛЕНПОЛІАМОНІЮ

Р. Є. Хома, К. В. Циганенко, Т. С. Бєньковська, Ю. В. Ішков, С. В. Водзінський

Одеський національний університет імені І. І. Мечникова,
вул. Дворянська, 2, Одеса 65082, Україна
email: rek@onu.edu.ua

В роботі наведено результати pH-, редокс- та кондуктометричного дослідження кислотно-основної взаємодії при хемосорбції діоксиду сірки водними розчинами на основі 0,1 моль/л цитратів моноетаноламонію (МЕА·1/3СА) та поліетиленполіамонію (РЕРА·1/3СА), а також буферними розчинами моноетаноламін – цитрат моноетаноламонію (МЕА·1/6СА) та поліетиленполіамін – цитрат поліетиленполіамонію (РЕРА·1/6СА) у порівнянні із цитратом натрію. Встановлено склад сполук, що утворюються при поглинанні SO_2 розчинами Na_3Cit, МЕА·1/3СА, РЕРА·1/3СА, МЕА·1/6СА, РЕРА·1/6СА при 273 – 313 К. За одних і тих самих значень кількості поглинутого діоксиду сірки) для розчинів SO_2–Na_3Cit–H_2O та SO_2–МЕА·1/3СА–H_2O відмічено збільшення значень питомої електропровідності (æ) з ростом температури при 273–313 К; значення Δæ зменшуються в системах SO_2–МЕА·1/3СА–H_2O, SO_2–РЕРА·1/3СА–H_2O, SO_2–МЕА·1/6СА–H_2O та SO_2–РЕРА·1/6СА–H_2O під час нагрівання при 283–303 К, що спричинено їхнім йон-молекулярним складом. На основі розроблених математичних моделей розраховано йон-молекулярний компонентний склад розчинів SO_2– МЕА·1/3СА–H_2O та SO_2–МЕА·1/6СА–H_2O при 283–313 К та концентраційні і термодинамічні константи утворення іонних асоціатів: $(NH_3CH_2CH_2OH)_2SO_3$, $\{\overset{+}{N}H_3CH_2CH_2OH\}\{HOC_3H_4(COOH)_2(COO^-)\}$ (**Ia**), $\{\overset{+}{N}H_3CH_2CH_2OH\}_2\{HOC_3H_4(COOH)(COO^-)_2\}$ (**IIa**), $\{\overset{+}{N}H_3CH_2CH_2OH\}_2\{HOC_3H_4(COOH)_2(COO^-)\}$ (**IIb**), $\{\overset{+}{N}H_3CH_2CH_2OH\}_3\{HOC_3H_4(COO^-)_3\}$ (**IIIa**), а також іон-молекулярних асоціатів $\{\overset{+}{N}H_3CH_2CH_2OH\}\{HOC_3H_4(COOH)_3\}$ (**Ib**), $\{NH_2CH_2CH_2OH\}_3\{\overset{+}{N}H_3CH_2CH_2OH\}_3\{HOC_3H_4(COO^-)_3\}$ (**IVa**), $\{NH_2CH_2CH_2OH\}_2\{\overset{+}{N}H_3CH_2CH_2OH\}_4\{HOC_3H_4(COO^-)_3\}$ (**IVb**).

У розчинах SO_2–МЕА·1/3СА–H_2O з ростом температури відбувається перегрупування зв'язків у іонних асоціатах **IIa** та **Ib**, на що вказує відсутність чіткої температурної залежності $p\beta^T_{IIIa}$, а також зміцнення сполук **IIa** та **Ib**. В розчинах SO_2–МЕА·1/6СА–H_2O з підвищенням температури відбувається послаблення зв'язків у сполуках **Ia**, **IIIa**, **IVa** та **IVb**, а у сполуці **Ib**, навпаки, посилення.

Ключові слова: діоксид сірки, амонієві цитрати, кислотно-основна взаємодія, іонні асоціати, іон-молекулярні асоціати.

REFERENCES

1. Hanif M.A., Ibrahim N., Abdul Jalil A. Sulfur dioxide removal: An overview of regenerative flue gas desulfurization and factors affecting desulfurization capacity and sorbent regeneration. *Environ. Sci. Pollut. Res.* 2020. **27**: 27515–27540.
doi: 10.1007/s11356-020-09191-4
2. Hou Y., Chen Y., He X., Wang F., Cai Q., Shen B. Insights into the adsorption of CO_2, SO_2 and NO_x in flue gas by carbon materials: A critical review. *Chem. Eng. J.* 2024. **490**: 151424.
doi: 10.1016/j.cej.2024.151424
3. Khoma R.E. Acid-base interaction and sulfooxidation at chemosorption of sulfur dioxide by alkylamines aqueous solutions. Abstract of Doctor's degree dissertation, 02.00.01. Kyiv, 2019, 50 p. (*in Ukrainian*).
4. Khoma R.E., Bienkovska T.S., Gelmboldt V.O., Klimov D.G., Horlichenko M.G. Composition and the relative stability of sulfur dioxide interaction products with potassium and monoethanolammonium taurates aqueous solutions. Prolonged-action chemosorbent. *Visn. Odes. nac. univ., Him.* 2023: **28**(3): 35–51.
doi: 10.18524/2304-0947.2023.3(86).297810.
(*in Ukrainian*).
5. Ennan A. A.-A., Khoma R.E., Dlubovskii R.M., Zukharenko Yu.S., Benkovska T.S., Knysh I.M. Mono- and bifunctional impregnated fiber chemosorbents for respiratory purpose. *Visn. Odes. nac. univ., Him.* 2022. **27**(1): 6–36.
doi: 10.18524/2304-0947.2021.4(80).248297.
(*in Ukrainian*).
6. Bekassy-Molnar E., Marki E., Majeed J.G. Sulphur dioxide absorption in air-lift-tube absorbers by sodium citrate buffer solution. *Chem. Eng. Process*. 2005. **44**(9): 1039–1046.
DOI: 10.1016/j.cep.2005.02.001
7. Jiang X., Liu Y., Gu M. Absorption of Sulfur Dioxide with Sodium Citrate Buffer Solution in a Rotating Packed Bed. *Chin. J. Chem. Eng.* 2011: **19**(4): 687–692.
doi: 10.1016/s1004-9541(11)60042-6
8. Sun Z., Zhou Y., Jia S., Wang Y., Jiang D., Zhang L. Enhanced SO_2 Absorption Capacity of Sodium Citrate Using Sodium Humate. *Catalysts*. 2021: **11**(7): 865.
doi: 10.3390/catal11070865
9. Khoma R.E., Bienkovska T.S., Tsyganenko K.V., Karych A.M., Kononchenko A.R. Acid-base and electrochemical behavior of monoethanolamine (polyethylenepolyamine) – citric acid – water solutions. *J. Chem. Technol.* 2024: **32**(1): 30–42.
doi: 10.15421/jchemtech.v32i1.292412.
(*in Ukrainian*).
10. Khoma R.E., Bienkovska T.S. Water vapor, sulfur dioxide and ammonia adsorption by fibrous material impregnated with citrate-monoethanolamine buffer solutions. *Visn. Odes. nac. univ. Him*. 2024: **29**(2):101–116.
doi: 10.18524/2304-0947.2024.2(88).322135.
(*in Ukrainian*).
11. Apelblat A. Citric acid. *Springer*. 2014. 357 p.
doi: 10.1007/978-3-319-11233-6
12. Verhoff F.H., Bauweleers H. Citric acid. in Ullmann's Encyclopedia Ind. Chem. 2014. 11 p.
doi: 10.1002/14356007.a07_103.pub3
13. Citric acid. Available at https://pubchem.ncbi.nlm.nih.gov/compound/Citric-Acid#section=Solubility
14. Apelblat A., Manzurola E. Extraction of Citric Acid by n-Octanol and n-Hexanol. Ber. *Bunsenges Phys. Chem.* 1988. **92**(7): 793–796.
doi: 10.1002/bbpc.198800195
15. *Sodium citrate*. EHS Support. 2021. 8 p. Available at https://www.santos.com/wp-content/uploads/2021/04/Sodium-citrate-March-2021.pdf

16. *Sodium Citrate, Dihydrate*. LabChem. Safety Data Sheet. 2020. 6 p. Available at https://ehslegacy.unr.edu/msdsfiles/36924.pdf
17. *Monoethanolamine*. Available at https://pubchem.ncbi.nlm.nih.gov/compound/Monoethanolamine#section=Carcinogen-Classification
18. *Polyamine B*. SDS AkzoNobel. 2014. 125 p. Available at https://www.alliancechemicals.com/wp-content/uploads/2011/10/Polyamine BSDS.pdf
19. *Polyethylene Polyamine*. Chem BK. Available at https://www.chembk.com/en/chem/Polyethylene%20Polyamine
20. Khoma R.E., Shestaka A.A., Gelmboldt V.O. On interaction of sulfur(IV) oxide with aqueous solutions of ethanolamines. *Russ. J. Appl. Chem.* 2012: **85**(11):1667–1675. doi: 10.1134/S1070427212110067
21. Hartley F.R., Burgess C., Alcock R.M. Solution Equilibria. Ellis Horwood Limited: Chichester, West Sussex, England. 1980. 361 p.

Стаття надійшла 05.01.2025.